Electrically, Chemically, and Photonically Powered Torsional and Tensile Actuation of Hybrid Carbon Nanotube Yarn Muscles

Márcio D. Lima *et al.*

Science **338**, 928 (2012);
DOI: 10.1126/science.1226762

Science (print ISSN 0036-8075; online ISSN 1095-9203) is published weekly, except the last week in December, by the American Association for the Advancement of Science, 1200 New York Avenue NW, Washington, DC 20005.

Electrically, Chemically, and Photonically Powered Torsional and Tensile Actuation of Hybrid Carbon Nanotube Yarn Muscles

Márcio D. Lima,[1*] Na Li,[1,2*] Mônica Jung de Andrade,[1] Shaoli Fang,[1] Jiyoung Oh,[1] Geoffrey M. Spinks,[3] Mikhail E. Kozlov,[1] Carter S. Haines,[1] Dongseok Suh,[1] Javad Foroughi,[3] Seon Jeong Kim,[4] Yongsheng Chen,[2] Taylor Ware,[1] Min Kyoon Shin,[4] Leonardo D. Machado,[5] Alexandre F. Fonseca,[6] John D. W. Madden,[7] Walter E. Voit,[1] Douglas S. Galvão,[5] Ray H. Baughman[1]†

Artificial muscles are of practical interest, but few types have been commercially exploited. Typical problems include slow response, low strain and force generation, short cycle life, use of electrolytes, and low energy efficiency. We have designed guest-filled, twist-spun carbon nanotube yarns as electrolyte-free muscles that provide fast, high-force, large-stroke torsional and tensile actuation. More than a million torsional and tensile actuation cycles are demonstrated, wherein a muscle spins a rotor at an average 11,500 revolutions/minute or delivers 3% tensile contraction at 1200 cycles/minute. Electrical, chemical, or photonic excitation of hybrid yarns changes guest dimensions and generates torsional rotation and contraction of the yarn host. Demonstrations include torsional motors, contractile muscles, and sensors that capture the energy of the sensing process to mechanically actuate.

The concept of deploying strong carbon nanotube yarns as actuators has produced both electrochemically and thermally powered yarn muscles. The performance of electrochemically powered yarn muscles (*1*, *2*) is adversely affected for most applications by the need for electrolyte, counter electrode, and device packaging, which add much more to actuator weight and volume than the actuating electrode. The electrolyte also limits operating temperature and voltage, as well as actuation rate. Previous work has demonstrated use of polymer-filled nontwisted carbon nanotube yarns as thermally powered shape memory actuators, but reversible actuation was not achieved (*3*). Dispersed carbon nanotubes and nanotube sheets have been used for electrically heating thermally actuating materials to provide cantilever deflections (*4*–*6*).

Here we demonstrate large-stroke, high-power, and high–work-capacity yarn muscles that provide millions of cycles and avoid the need for electrolyte or special packaging. Torsional and tensile actuation of these hybrid muscles results from dimensional changes of a yarn guest. The twist-spun nanotubes confine this actuating guest in both solid and molten states and provide the mechanical strength and helical geometry enabling large-stroke torsional and tensile actuation. Reversible actuation is powered electrically, photonically, or by chemical absorption and desorption.

Yarn fabrication and structure. Nanotubes drawn from a carbon multiwall nanotube (MWNT) forest are twist-spun into a yarn (*7*–*14*). The utilized forests are ~350 μm high and consist of MWNTs that have an outer diameter of ~9 nm, contain about six walls, and form large bundles. Symmetric twist insertion during sheet draw from a forest or into a predrawn nanotube sheet (suspended between either a forest and one rigid support or two rigid supports) provides the two investigated helical yarn structures (Fermat scrolls for the former cases and dual-Archimedean scrolls for the latter) (*15*, *16*) illustrated in Fig. 1, H and I. The bias angle (the angle between the yarn length and nanotube directions) for the simpler Fermat yarn is

$$\alpha = \tan^{-1}(2\pi r T) \quad (1)$$

where r is the distance from yarn center and T is the inserted twist in turns per yarn length. The measured bias angle is that for the yarn surface, where r equals the yarn radius. Overtwisting these MWNT yarns, as for ordinary textile yarns, rubber bands, and DNA molecules, causes coiling, which is called writhe (*17*–*20*). This coiling, as well as coiling in plied yarn, will be used to dramatically amplify tensile stroke and work capabilities compared with those for uncoiled yarn (*21*).

Methods for incorporating guest actuating material into the host yarn include melt and solution infiltration (which can be followed by in situ polymerization) and biscrolling, in which the guest is deposited on a MWNT sheet before twist insertion.

Nanotube muscle chirality and tethering. Yarn volume during actuation for nonplied hybrid

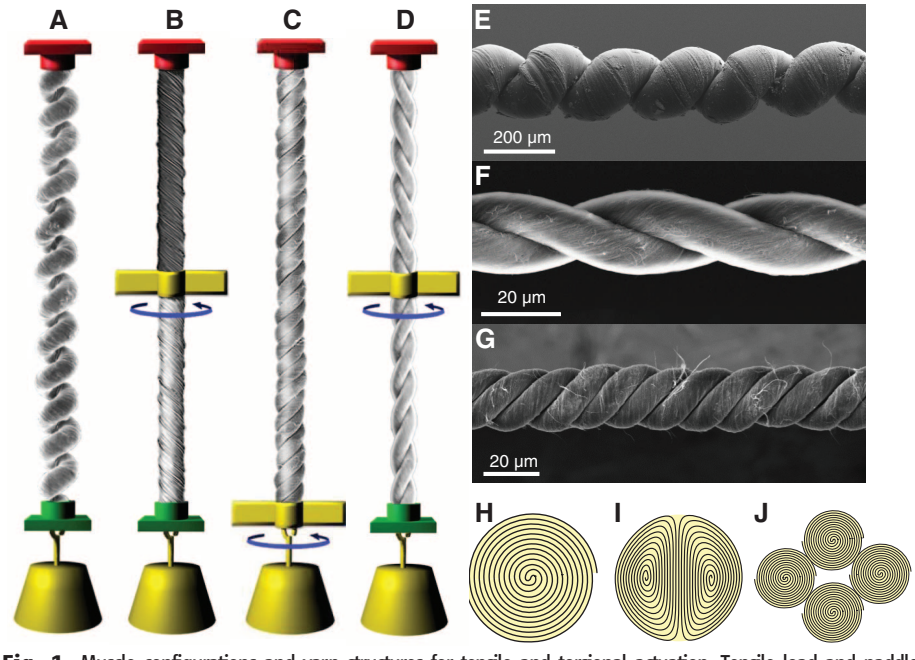

Fig. 1. Muscle configurations and yarn structures for tensile and torsional actuation. Tensile load and paddle positions for (**A**) a two-end–tethered, fully infiltrated homochiral yarn; (**B**) a two-end–tethered, bottom-half–infiltrated homochiral yarn; (**C**) a one-end–tethered, fully infiltrated homochiral yarn; and (**D**) a two-end–tethered, fully infiltrated heterochiral yarn. The depicted yarns are coiled, noncoiled, four-ply, and two-ply, respectively. Arrows indicate the observed direction of paddle rotation during thermal actuation. Red and green yarn-end attachments are tethers, meaning they prohibit end rotation; red attachments also prohibit translational displacement. SEM micrographs of (**E**) a fully infiltrated homochiral coiled yarn, (**F**) a neat two-ply yarn, and (**G**) a neat four-ply yarn. Illustration of ideal cross sections for (**H**) Fermat, (**I**) dual-Archimedean, and (**J**) infiltrated four-ply Fermat yarns.

[1]The Alan G. MacDiarmid NanoTech Institute, University of Texas at Dallas, Richardson, TX 75083, USA. [2]Centre of Nanoscale Science and Technology, Institute of Polymer Chemistry, College of Chemistry, Nankai University, Tianjin 300071, China. [3]Intelligent Polymer Research Institute, Australian Research Council Centre of Excellence for Electromaterials Science, University of Wollongong, Wollongong, NSW 2522, Australia. [4]Center for Bio-Artificial Muscle and Department of Biomedical Engineering, Hanyang University, Seoul 133-791, South Korea. [5]Applied Physics Department, State University of Campinas, Campinas, SP, 13081-970, Brazil. [6]Faculdade de Ciências, Universidade Estadual Paulista, Bauru, SP, 17033-360, Brazil. [7]Department of Electrical and Computer Engineering, University of British Columbia, Vancouver, BC V6T 1Z4, Canada.

*These authors contributed equally to this work.
†To whom correspondence should be addressed: E-mail: ray.baughman@utdallas.edu

yarns (i.e., yarns that are not wrapped around another yarn) causes tensile contraction and untwist. Since the untwisting of a nonplied actuating yarn segment causes elongation that partially cancels yarn contraction, maximizing tensile contraction and torsional actuation generally require different configurations.

We predict configurations that optimize either torsional or tensile actuation for yarns, where the only variables are whether guest infiltration is along the entire yarn or one-half its length, whether the yarn is homochiral (one chirality) or heterochiral (with equal length segments having opposite chirality), and whether the yarn is nonplied or plied. Using opposite chirality, nonplied yarn segments (designated S and Z), with a paddle at their interconnection (Fig. 1D), maximizes initial torque on the paddle, because these segments operate additively to provide rotation. For the same yarn, the one-end–tethered configuration of Fig. 1C provides twice the torsional rotation of the Fig. 1D configuration, but one-half the initial torque, so both configurations provide equal torsional work capacity. Actuation of one segment in a two-end–tethered homochiral yarn (Fig. 1B) generates smaller rotation than for the heterochiral yarn of Fig. 1D because of the energetic cost of twisting the unactuated yarn as the actuating yarn untwists. As with the Fig. 1C configuration, the Fig. 1D configuration with nonplied yarn does not provide reversible actuation unless internally constrained by a solid guest, to prevent S twist from canceling Z twist in the other yarn segment.

Yarn untwist is prohibited in Fig. 1A unless symmetry is broken for energetic reasons to provide yarn segments with opposite changes in twist, while untwist of the actuating segment is compensated by up-twist of the nonactuated segment in Fig. 1B, so these actuator configurations can optimize tensile contraction per length for a nonplied actuated yarn. Because the entire yarn untwists for the Fig. 1, C and D, configurations during actuation when the yarn is nonplied, they do not provide optimized tensile contraction.

Thermally, electrothermally, and photothermally powered actuation. Thermal actuation of hybrid yarn muscles is largely driven by volume expansion of the yarn guest. Paraffin waxes are used as prototypical guests because of high thermal stability; the tunability of transition widths and temperatures; the large volume changes associated with phase transitions and thermal expansion; and their ability to wet carbon nanotube yarns. Such waxes have been long investigated and commercially deployed as thermally or electrothermally powered actuators (*22*). By confining the actuating wax in the nanosized pores of a MWNT yarn (fig. S3), the goal is to avoid conventional hydraulic and external heating systems and directly use a muscle-like geometry, where high surface/volume and thermal and electrical conductivities enhance response rate and a helical geometry enables both torsional rotation and tensile contraction. Results described are for a commercial wax ("Aldrich wax," Sigma Aldrich 411671), which fully melts at ~83°C, increases volume ~20% between 30° and 90°C, and expands an additional ~10% between 90° and 210°C (fig. S5).

Tensile contraction versus temperature for coiled dual-Archimedean yarn, before and after wax infiltration, is compared in Fig. 2A with corresponding data (figure inset) for noncoiled Fermat yarn. Wax infiltration greatly enhanced tensile contraction for all yarns, as did yarn coiling. Despite a difference in the load dependence of actuation, similar tensile strokes were obtained for noncoiled, Fermat, and dual-Archimedean yarns having similar diameter and twist angle (fig. S2). Heating the neat coiled yarn from ambient to incandescent temperature (~2560°C) under 3.8-MPa tensile stress provided a reversible yarn contraction of 7.3% (Fig. 2B and movie S4), corresponding to 0.16 kJ/kg of contractile work capability per yarn weight. Because yarn coiling greatly enhanced actuation stroke, coiled yarns (Fig. 1E) are the focus of the studies on tensile actuation discussed below.

Tensile actuation at 1200 cycles per minute and 3% stroke was demonstrated for more than 1.4 million cycles (Fig. 3A) with a two-end–tethered, wax-filled, coiled Fermat yarn that lifted 17,700 times its own weight when powered by a 20-Hz, 18.3-V/cm square-wave voltage. Fast passive cooling in 25 ms resulted from the small yarn and coil diameters (11.5 and 20 μm, respectively). The performance of this yarn was optimized by increasing applied voltage and mechanical load, while reducing pulse duration. Figure 3B shows a series of actuations wherein the yarn lifts 175,000 times its mass in 30 ms when 32 V/cm was applied for 15 ms. The work during contraction (0.836 kJ/kg) provided a power output of 27.9 kW/kg, which is 85 times the peak output of mammalian skeletal muscles (0.323 kW/kg) (*23*) and 30 times the maximum measured power density of previous carbon nanotube muscles. However, the high applied electrical power reduces cycle life by causing excessive heating and paraffin evaporation.

Figure 3C shows the stress dependence of actuator stroke and work capacity for different amounts of twist insertion in a wax-infiltrated, 150-μm-diameter, dual-Archimedean yarn that is two-end tethered. Reversible contraction, which is greatly enhanced for yarn having sufficient twist to cause coiling, resulted from steady-state electrical heating to just below the wax vaporization temperature. Applying high stress decreases stroke, owing to the yarn's lower Young's modulus in the contracted state (containing molten wax)

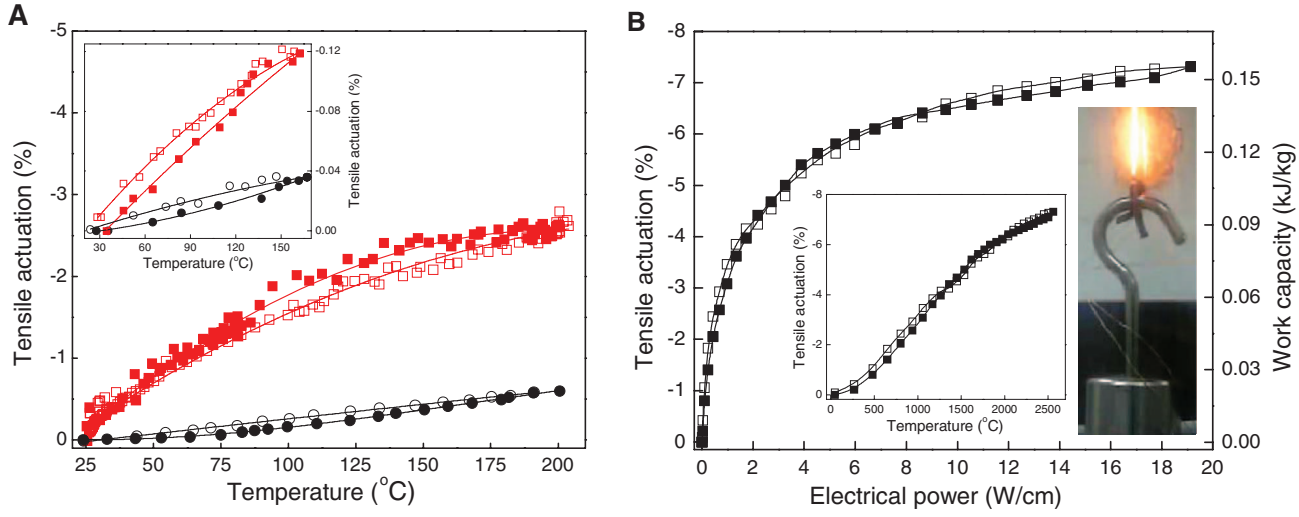

Fig. 2. Thermal tensile actuation for two-end–tethered homochiral yarns. (**A**) Tensile actuation strain versus temperature before (black) and after (red) wax infiltration for a coiled, dual-Archimedean yarn having 130-μm initial diameter, an inserted twist of ~4000 turns/m (per length of the precursor sheet stack), and an applied stress of 6.8 MPa. Inset: Corresponding actuation data before (black) and after (red) wax infiltration for a noncoiled Fermat yarn having 16-μm initial diameter, ~20,000 turns/m twist, and an applied stress of 4.8 MPa. (**B**) Electrothermal tensile actuation strain and work capacity during contraction in vacuum as a function of applied electrical power for a neat, coiled, dual-Archimedean yarn having 115-μm diameter and the inserted twist of the dual-Archimedean yarn in (A). Insets: Tensile actuation versus estimated temperature for this yarn (left) and photograph of the incandescent yarn lifting a 10-g load. Closed symbols and open symbols in (A) and (B) are for increasing and decreasing temperature, respectively.

and correspondingly larger elastic elongation under load than in the initial state (where the solid wax provides structural reinforcement for both tensile and torsional deformations) (fig. S2). The stroke for highly coiled yarn decreases at low stresses (Fig. 3C), which is consistent with the close proximity of adjacent coils hindering contraction.

Figure 3C shows that there is an optimal amount of coiling that maximizes either stroke or work during contraction for the wax hybrid yarn. A maximum contraction of 5.6% was observed at 5.7-MPa stress for a coiled Fermat yarn having intermediate twist. Adding 6.8% more twist to the coiled yarn increased the stress of maximum contraction (16.4 MPa for 5.1% strain) and the maximum measured contractile work (1.36 kJ/kg at 84 MPa), which is 29 times the work capacity of natural muscle (*24*). Subsequently reducing twist by 41% eliminated coiling and reduced maximum contraction and contractile work to low values (0.7% and 0.31 kJ/kg, respectively). Contractions of 10% under 5.5-MPa stress were realized for a 150-μm-diameter, partially coiled, dual-Archimedean yarn by applying well-separated 50-ms, 15-V/cm pulses (Fig. 3D). Because the cross-sectional area of this yarn was 170 times higher than for the yarn of Fig. 3, A and B, passive cooling in ambient air was less effective: The cooling time increased from 25 ms to ~2.5 s, resulting in a low contractile power density when both heating and cooling times are considered (0.12 kW/kg).

The highest presently realized ratio of the mechanical work done during contraction to the input electrical energy is 0.55% (*25*), which is similar to the energy conversion efficiency of commercially used shape memory metals, which can reach 1 or 2% (*26*). The energy efficiency for the hybrid yarn muscles can be increased by minimizing the thermal energy loss during actuation, increasing the allowable mechanical load by increasing yarn strength, and increasing the ratio of guest volume change to the enthalpy change needed to produce it.

The Fig. 1, C and D, configurations provided highly reversible torsional and tensile actuation when the final actuation temperature (T_f) was below the temperature at which wax melting starts (T_{ms}). Actuation for these configurations became increasingly irreversible at higher temperatures for nonplied yarn, especially when mechanical load was large, and cycling to above T_{mf} (where melting is complete) caused large permanent untwist. This problem does not arise for SZ two-ply yarn (or its chiral opposite); because the sum of yarn Z twist and the S twist of yarn plying must be conserved, uncoiling during reversal of actuation acts as a torsional return spring for reversing twist release within the yarn (*27*) (fig. S9).

Very fast, highly reversible torsional actuation was demonstrated for 2 million cycles for a 6.9-cm-long, 10-μm-diameter, two-end–tethered, half-wax–infiltrated homochiral Fermat yarn that rotated a paddle at yarn midpoint (Fig. 1B configuration). The hybrid yarn accelerated a 16.5-times-heavier paddle to a full-cycle–averaged 11,500 rotations per minute—first in one direction and then in reverse (Fig. 4A). Even though actuation temperature was far above T_{mf}, this high cycle life resulted because of the presence of the unactuated yarn segment of Fig. 1B, whose twisting during the untwisting of the actuating yarn segment acted as a torsional return spring. Figure 4B shows the dependence of torsional rotation on input electrical power and applied tensile load for a similar yarn that rotated a 150-times-heavier paddle for a million highly reversible cycles. Increasing load increased rotation speed from 5500 revolutions/minute (movie S2) to a maximum of 7900 revolutions/minute. Reversible torsional actuation (12.6°/mm) was also driven for a half-wax–infiltrated yarn by replacing electrical heating with heating using light pulses (movie S4) from a 100-W incandescent lamp.

Torsional actuation of a fully infiltrated, heterochiral, noncoiled, dual-Archimedean yarn (Fig. 1D) was used to hurl a projectile by rotating the arm of a miniature Greco-Roman–style catapult by 300° (Fig. 4C and movie S3). A maximum specific torque of 8.42 N·m/kg was generated for this 100-μm-diameter yarn, which is five times the value demonstrated for electrochemically driven nanotube yarn and slightly higher than for large electric motors (up to 6 N·m/kg). Though the maximum torsional actuation temperature was above T_{mf} and the yarn is heterochiral and fully infiltrated, reversible operation was achieved as the torsional rotation range was limited to 130° and the actuation temperature was below that of appreciable wax evaporation.

We have also demonstrated reversible, thermally powered torsional actuation for hybrid yarn containing other volume-expanding guests. One example is $CH_3(CH_2)_{11}C{\equiv}C\text{-}C{\equiv}C(CH_2)_8COOH$, which was infiltrated into twist-spun Fermat yarn (diameter = 9 μm and α = 30°) and photopolymerized by 1,4-addition. Similar to a related polydiacetylene used to make color-changing carbon nanotube yarns (*28*), the produced polydiacetylene is polychromatic, providing a reversible blue-to-red phase transition at ~57°C. Owing to a few percent volume increase at this blue-red phase transition and a larger volume change from melting incompletely polymerized monomer at 63°C,

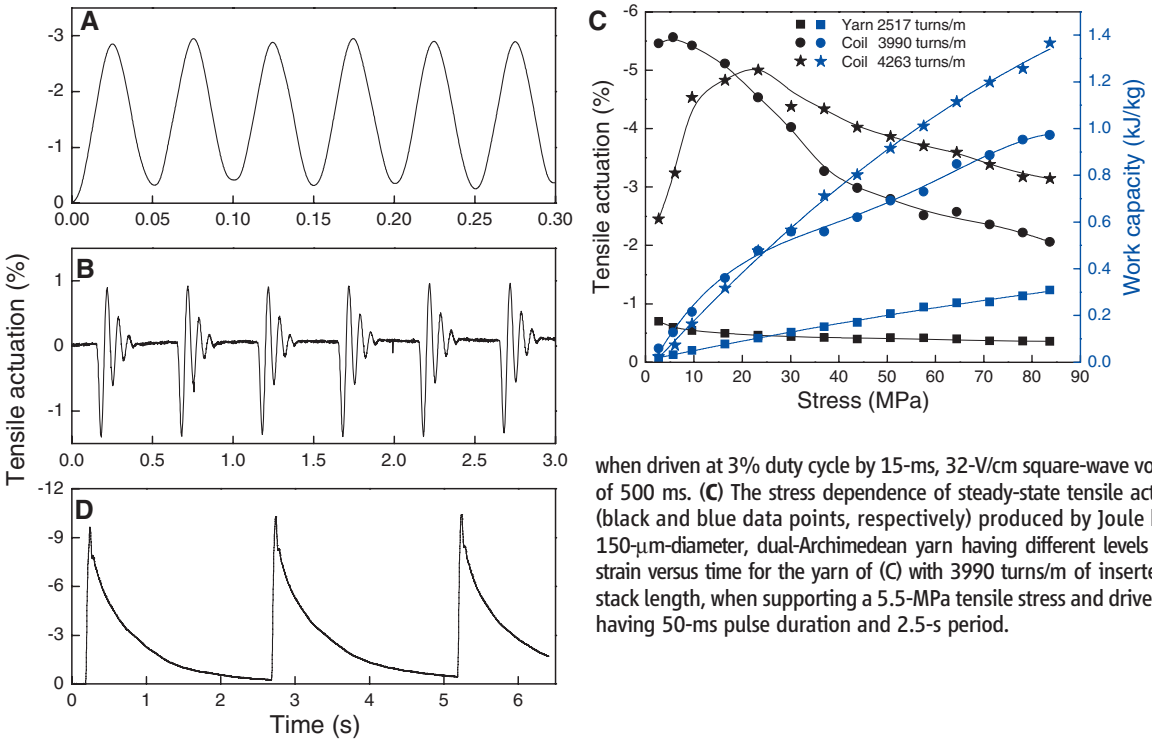

Fig. 3. Electrothermal tensile actuation for two-end–tethered, homochiral, wax-filled yarns. (**A**) Tensile actuation strain versus time after 1,400,000 reversible cycles for a 11.5-μm-diameter, coiled Fermat yarn having ~25,000 turns/m twist when driven by an 18.3-V/cm, 20-Hz symmetric square wave voltage while lifting a load that provided a 14.3-MPa stress. (**B**) Tensile actuation for the yarn of (A) with 109-MPa applied tensile stress when driven at 3% duty cycle by 15-ms, 32-V/cm square-wave voltage pulses having a period of 500 ms. (**C**) The stress dependence of steady-state tensile actuation and contractile work (black and blue data points, respectively) produced by Joule heating (0.189 V/cm) for a 150-μm-diameter, dual-Archimedean yarn having different levels of inserted twist. (**D**) Tensile strain versus time for the yarn of (C) with 3990 turns/m of inserted twist per precursor sheet stack length, when supporting a 5.5-MPa tensile stress and driven by a 15-V/cm square wave having 50-ms pulse duration and 2.5-s period.

reversible torsional rotation of 100°/mm was obtained for actuation to below 80°C for the yarn configuration of Fig. 1B. Actuation to higher temperatures was poorly reversible, likely because of an irreversible phase transition.

Actuation powered by absorption. Reversible torsional actuation was powered by the absorption and desorption of hydrogen on a 60-nm-thick palladium layer on nanotube bundles (fig. S4) within a dual-Archimedean yarn (*16*). Because this 144-μm-diameter yarn contained 90 weight (wt) % palladium, the resulting high torsional rigidity restricted twist insertion to ~200 turns/m. Nevertheless, a one-end–tethered yarn rotated at its free end a thousand-times-heavier paddle during hydrogen absorption. Injection of 0.05-atm H_2 into a vacuum chamber containing the actuator caused 1.5 paddle rotations within ~6 s, which was fully reversed on a similar time scale during repeated cycling between hydrogen exposure and vacuum. Cantilever-based actuators exploiting the dimensional changes of a 10-μm-thick Pd alloy layer have been previously demonstrated (*29*), but the response time was in tens of minutes. The yarn's 100-fold faster response rate resulted from yarn porosity and the thinness of the Pd coating. Such yarn actuators might be used as intelligent muscles that rapidly close an inlet when a targeted hydrogen pressure is exceeded.

Liquid absorption and desorption can also drive actuation, as shown in fig. S10, where torsional actuation of a two-end–tethered Fermat yarn is shown as a function of immersion length in liquid. As with a polymer that absorbs a liquid or vapor, the immersed yarn swells, and this volume change drives torsional actuation.

Discussion. The volume expansion of a liquid wax reversibly drives actuation rather than causing wax extrusion from the porous yarn because of the giant interfacial energies that arise on the nanoscale. The molten wax undergoes a fractional volume decrease $\Delta V_w/V_w$ when cooled. If this wax volume change occurred without decreasing yarn volume, nanotube-paraffin interfacial energies (γ_{np}) would be replaced by nanotube-air interfacial energies (γ_{na}) at an energy cost of $(\gamma_{na} - \gamma_{np})(\Delta V_w/V_w)A_n$, where A_n is the gravimetric surface area of the nanotubes. Using $\gamma_{na} - \gamma_{np} \sim 18$ mJ/m^2 (*30*), $A_n \sim 97$ m^2/g (*31*), and $\Delta V_w/V_w \sim 0.2$, about 0.35 kJ/kg of energy is available to compress the nanotube yarn as the volume of the liquid wax decreases. During subsequent yarn actuation by heating and corresponding wax expansion, this elastic energy in the yarn is progressively released, thereby maintaining coincidence between molten wax and yarn volume over the entire actuation cycle—as is observed. This analysis correctly predicts that excess wax on the yarn surface, as well as wax evaporation, will decrease tensile stroke.

Why is tensile contraction no more than 0.7% for wax-filled, noncoiled, nonplied yarns undergoing volume expansions of about 10% (fig. S2), despite these same yarns providing high torsional actuation? Low tensile contraction results for a noncoiled, Fermat yarn because the yarn bias angle decreases toward zero with decreasing radius within the yarn (Eq. 1) and the fractional contraction ($\Delta L/L$) produced by a fractional volume change strongly depends upon bias angle (fig. S11). Length contraction of the outer yarn layer is dramatically reduced by dimensional mismatch with progressively smaller contractions closer to yarn center. This dimensional mismatch similarly limits tensile contraction for the component helical scrolls in dual-Archimedean yarn.

The thermal expansion coefficient for noncoiled, neat, Fermat yarn between 25° and 200°C (about -2.2×10^{-6}/°C) (Fig. 2A, inset) is similar to the in-plane thermal expansion coefficient of graphite (which has a minimum of -1.4×10^{-6}/°C at about 3°C, increases to -0.71×10^{-6}/°C at 200°C, and becomes positive above ~380°C) (*32*). However, the tensile contraction of uncoiled neat yarn becomes 2.8 times as negative with increasing twist (fig. S1), indicating that contraction of nanotube length cannot fully explain yarn contraction. This yarn contraction is relatively insensitive to mechanical load and is approximately the same for

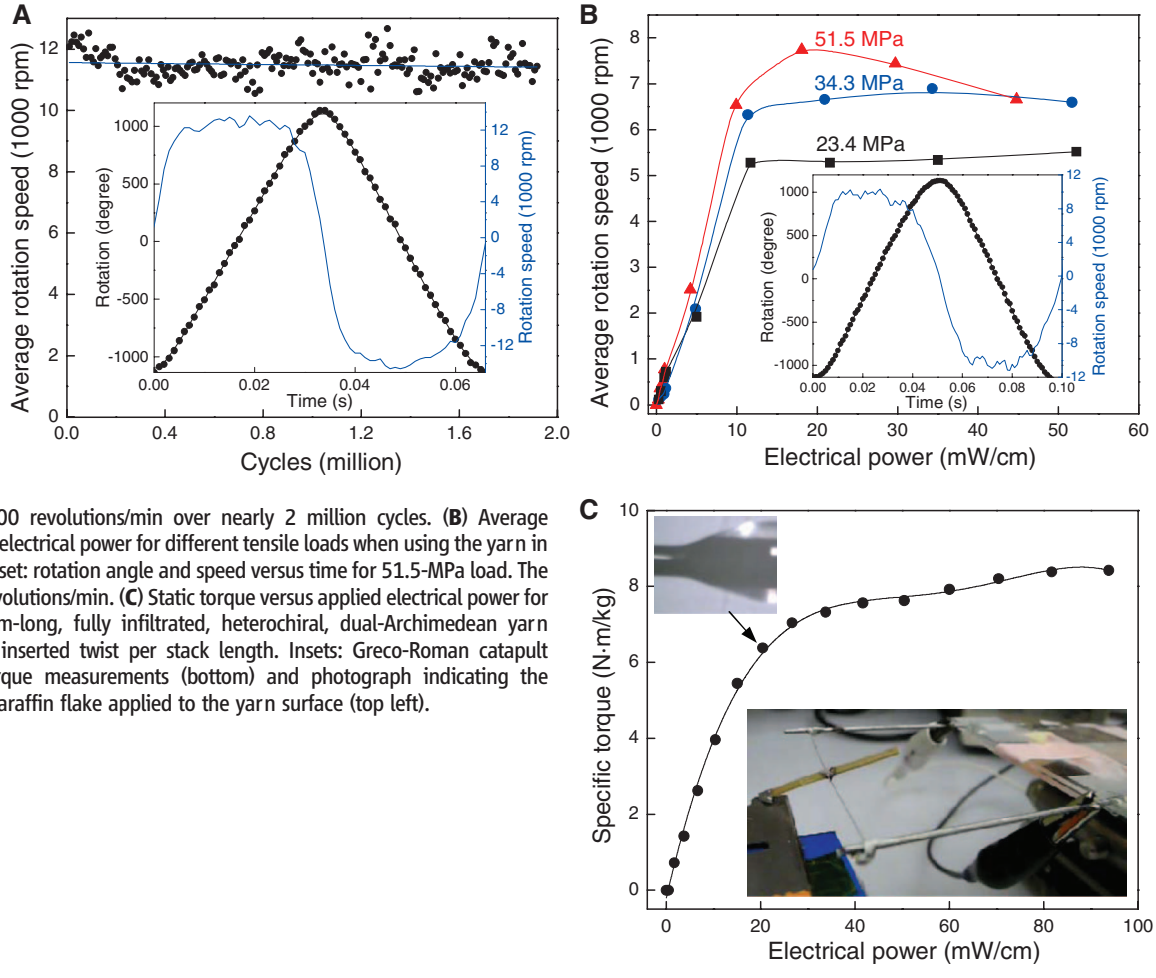

Fig. 4. Torsional actuation for two-end–tethered, wax-infiltrated yarns. (**A**) Average rotation rate versus cycle number for a 6.9-cm-long, half-infiltrated, homochiral Fermat yarn (10 μm diameter and ~22,000 turns/m twist), when excited by a 15-Hz, 40-V/cm, square-wave voltage using 50% duty cycle and 41-MPa applied load. Each point on the graph is the average speed over 120 cycles. Inset: rotation angle and rotation speed versus time for one complete cycle. The average rotation speed was ~11,500 revolutions/min over nearly 2 million cycles. (**B**) Average rotation rate versus applied electrical power for different tensile loads when using the yarn in (A) and a heavier paddle. Inset: rotation angle and speed versus time for 51.5-MPa load. The average speed was 7600 revolutions/min. (**C**) Static torque versus applied electrical power for a 100-μm-diameter, 6.4-cm-long, fully infiltrated, heterochiral, dual-Archimedean yarn having ~3000 turns/m of inserted twist per stack length. Insets: Greco-Roman catapult configuration used for torque measurements (bottom) and photograph indicating the melting temperature of a paraffin flake applied to the yarn surface (top left).

neat Fermat and dual-Archimedean yarns having about the same diameter and bias angle (fig. S2).

Diverse structural effects can potentially contribute to tensile actuation for coiled, two-end–tethered, nonplied yarns, including conversion between twist and writhe (in both uncoiled and coiled regions) and changes in coil diameter, pitch, and yarn length. Although twist-to-writhe conversion (corresponding to an increase in number of coils) would enhance thermal contraction during actuation, optical microscopy indicates that total coil number does not measurably increase during actuation for either heavily or lightly coiled, wax-filled, dual-Archimedean yarns. These results suggest that tensile contraction is predominantly caused by a decrease in separation between neighboring coils.

Yarn coiling increases the negative thermal expansion of a neat twist-spun yarn by a factor of ~10. Because these coiled neat yarns provide up to 7.3% hysteresis-free contraction when lifting heavy loads using temperature changes up to ~2560°C (Fig. 2B and movie S4), these muscles can be deployed in inert atmosphere to temperatures at which no other high–work-capacity actuator can survive.

For applications in which yarn-size torsional and tensile actuators are needed, the absence of electrolyte and associated packaging, the low required voltages, and the high cycle life and energy and power densities suggest the possibility of early commercial deployment. The main competing technology of NiTi shape memory metal actuators provides highly hysteretic actuator strokes; actuator control is complicated by the dependence of stroke on prior history within a cycle (*26*). This history dependence is small for the wax hybrid yarn results of Fig. 2A and should be negligible for cycling a neat yarn or any wax-filled yarn between molten states. However, as with shape memory metal wires and other thermally powered actuators (*26*), electrothermal energy conversion efficiency is low. Future possibilities include environmentally powered hybrid muscles that open textile pores or close window blinds when it is too hot, or actuate in response to agents in the environment.

References and Notes

1. T. Mirfakhrai *et al.*, *Smart Mater. Struct.* **16**, S243 (2007).
2. J. Foroughi *et al.*, *Science* **334**, 494 (2011).
3. P. Miaudet *et al.*, *Science* **318**, 1294 (2007).
4. A. T. Sellinger, D. H. Wang, L.-S. Tan, R. A. Vaia, *Adv. Mater. (Deerfield Beach Fla.)* **22**, 3430 (2010).
5. L. Chen *et al.*, *ACS Nano* **5**, 1588 (2011).
6. Y. Hu, W. Chen, L. H. Lu, J. H. Liu, C. R. Chang, *ACS Nano* **4**, 3498 (2010).
7. M. Zhang, K. R. Atkinson, R. H. Baughman, *Science* **306**, 1358 (2004).
8. M. Zhang *et al.*, *Science* **309**, 1215 (2005).
9. X. Zhang *et al.*, *Adv. Mater.* **18**, 1505 (2006).
10. Q. Li *et al.*, *Adv. Mater.* **18**, 3160 (2006).
11. X. Zhang *et al.*, *Small* **3**, 244 (2007).
12. L. Xiao *et al.*, *Appl. Phys. Lett.* **92**, 153108 (2008).
13. Y. Nakayama, *Jpn. J. Appl. Phys.* **47**, 8149 (2008).
14. M. B. Jakubinek *et al.*, *Carbon* **50**, 244 (2012).
15. M. D. Lima *et al.*, *Science* **331**, 51 (2011).
16. Materials and methods are available as supplementary materials on *Science* Online.
17. F. B. Fuller, *Proc. Natl. Acad. Sci. U.S.A.* **68**, 815 (1971).
18. A. Goriely, M. Tabor, *Physica D* **105**, 20 (1997).
19. A. F. da Fonseca, C. P. Malta, D. S. Galvão, *J. Appl. Phys.* **99**, 094310 (2006).
20. Y. Shang *et al.*, *Adv. Mater.* **24**, 2896 (2012).
21. The presently used term "inserted twist" (which is sometimes called linking number) is the sum of internal yarn twist and the twist due to coiling. As done for other structural terms, "yarn diameter" refers to the diameter of the component yarn even when it is within a coiled or plied structure, and is thereby differentiated from the "coiled yarn diameter" or the "plied yarn diameter."
22. E. T. Carlen, C. H. Mastrangelo, *J. Microelectromech. Syst.* **11**, 165 (2002).
23. R. K. Josephson, *Annu. Rev. Physiol.* **55**, 527 (1993).
24. D. R. Peterson, J. D. Bronzino, *Biomechanics: Principles and Applications* (CRC Press, Boca Raton, FL, 2008).
25. This efficiency was measured in the Fig. 1A configuration for 1.5% actuation of a coiled, wax-filled, 150-μm-diameter, dual-Archimedean yarn using a 1-ms electrical pulse and 55-MPa applied stress. Full contraction occurred within ~30 ms of pulse start.
26. J. E. Huber, N. A. Fleck, M. F. Ashby, *Proc. R. Soc. Lond. A* **453**, 2185 (1997).
27. To understand this conversion of yarn twist to twist due to yarn plying, overtwist a yarn and fold it back on itself. The yarn will automatically become two ply as the initial inserted twist is partially converted to plying in the opposite twist direction.
28. H. Peng *et al.*, *Nat. Nanotechnol.* **4**, 738 (2009).
29. M. Mizumoto, T. Ohgai, A. Kagawa, *J. Alloy. Comp.* **482**, 416 (2009).
30. P. Pötschke, S. Pegel, M. Claes, D. Bonduel, *Macromol. Rapid Commun.* **29**, 244 (2008).
31. R. Zhou *et al.*, *Nanotechnology* **21**, 345701 (2010).
32. B. T. Kelley, *Carbon* **29**, 721 (1991).

Acknowledgments: We thank X. Lepró for scanning electron micrograph (SEM) images of yarn cross sections; B. J. Swedlove, D. B. Hagenasr, J. M. Cruciger, C. Mozayan, and S. Rudraraju for assistance with sample preparation and measurements; and F. Göktepe and Ö. Göktepe for valuable discussions. Support is largely from Air Force Office of Scientific Research grants FA9550-09-1-0537 and FA9550-12-1-0211, with additional support from Office of Naval Research MURI grant N00014-08-1-0654, Robert A. Welch Foundation grant AT-0029, the Creative Research Initiative Center for Bio-Artificial Muscle and the Korea–U.S. Air Force Cooperation Program grant-2012-00074 (Korea), and the Centre of Excellence funding from the Australian Research Council. N.L. and Y.C. acknowledge financial support from MoST (grant 2012CB933401) and National Natural Science Foundation of China (grant 50933003). D.S.G., L.D.M., and A.F.F. are research fellows of the Conselho Nacional de Desenvolvimento Científico e Tecnológico and the Fundação de Amparo à Pesquisa do Estado de São Paulo of Brazil. A provisional patent application on the topic of this manuscript has been filed by N. Li *et al.*, "Coiled and non-coiled nanofiber yarn torsional and tensile actuators," U.S. Provisional Patent 61678340 (1 August 2012).

Supplementary Materials

www.sciencemag.org/cgi/content/full/338/6109/928/DC1
Supplementary Text
Figs. S1 to S11
References (*33*–*37*)
Movies S1 to S5

2 July 2012; accepted 13 September 2012
10.1126/science.1226762

REPORTS

Synthetic Lipid Membrane Channels Formed by Designed DNA Nanostructures

Martin Langecker,[1]* Vera Arnaut,[1]* Thomas G. Martin,[2]* Jonathan List,[1] Stephan Renner,[1] Michael Mayer,[3] Hendrik Dietz,[2]† Friedrich C. Simmel[1]†

We created nanometer-scale transmembrane channels in lipid bilayers by means of self-assembled DNA-based nanostructures. Scaffolded DNA origami was used to create a stem that penetrated and spanned a lipid membrane, as well as a barrel-shaped cap that adhered to the membrane, in part via 26 cholesterol moieties. In single-channel electrophysiological measurements, we found similarities to the response of natural ion channels, such as conductances on the order of 1 nanosiemens and channel gating. More pronounced gating was seen for mutations in which a single DNA strand of the stem protruded into the channel. Single-molecule translocation experiments show that the synthetic channels can be used to discriminate single DNA molecules.

A large class of proteins and peptides form channels through lipid bilayer membranes (*1*) to facilitate the transport of water, ions, or other entities through the otherwise impermeable membranes. Here, we report on a synthetic membrane channel that is constructed entirely from DNA and anchored to a lipid membrane by cholesterol side chains. The shape of our synthetic channel is inspired by the natural channel protein α-hemolysin (*2*), although there are differences in physical properties such as charge, hydrophobicity, and size.

We constructed the channel by means of molecular self-assembly with scaffolded DNA origami (*3*–*9*) (Fig. 1A). The channel consists of two modules: (i) a stem that penetrates and spans a lipid membrane, and (ii) a barrel-shaped cap

[1]Lehrstuhl für Bioelektronik, Physics Department and ZNN/WSI, Technische Universität München, 85748 Garching, Germany. [2]Walter Schottky Institute, Physics Department, Technische Universität München, 85748 Garching, Germany. [3]Department of Biomedical Engineering, University of Michigan, Ann Arbor, MI 48109, USA.

*These authors contributed equally to this work.
†To whom correspondence should be addressed. E-mail: dietz@tum.de (H.D.); simmel@tum.de (F.C.S.)